Research Square

Preprints are preliminary reports that have not undergone peer review.
They should not be considered conclusive, used to inform clinical practice,
or referenced by the media as validated information.

Study on the evolution law and numerical simulation of the mechanical properties of rockfill under dry-wet cycle conditions

Rongxian Yang
Xinjiang Agricultural University
Lingkai Zhang
xjauzhanglk@163.com

Xinjiang Agricultural University
Chong Shi
Xinjiang Agricultural University
Runhan Zhang
Xinjiang Agricultural University

Research Article

Keywords: Dry-wet cycle, Rockfill, Discrete element method, Mechanical properties, micrscopic mechanism

Posted Date: September 19th, 2025

DOI: https://doi.org/10.21203/rs.3.rs-7467471/v1

License: This work is licensed under a Creative Commons Attribution 4.0 International License.
Read Full License

Additional Declarations: No competing interests reported.

Version of Record: A version of this preprint was published at Granular Matter on January 29th, 2026.
See the published version at https://doi.org/10.1007/s10035-025-01608-6.

Study on the evolution law and numerical simulation of the mechanical properties of rockfill under dry-wet cycle conditions

Rongxian Yang[1,2], Lingkai Zhang[*1,2], Chong Shi[1,2,3], Runhan Zhang[1,2]

1. College of Hydraulic and Civil Engineering, Xinjiang Agricultural University, Urumqi 830052, China

2. Xinjiang Key Laboratory of Hydraulic Engineering Security and Water Disasters Prevention, Urumqi 830052, China

3. Geotechnical Reserch Institute, Hohai University, Nanjing, Jiangsu 210024, China

*Corresponding author Lingkai Zhang, E-mail: xjauzhanglk@163.com

Abstract

The mechanical properties of rockfill materials degrade markedly under dry-wet cycles, uneven settlement of rockfill dams over time. This study employed numerical simulations of crushable triaxial compression on rockfill samples subjected to various dry-wet cycles, utilizing the particle discrete element method. The macroscopic mechanical behavior and the micrscopic degradation mechanisms of rockfill under these cycles were subsequently analyzed. The research findings are presented in detail below: **(1) Macroscopic law:** As the number of dry-wet cycles (N) increases, the peak stress of rockfill decreases while the volume strain increases. After N reaches a certain threshold, the peak stress and volume strain show minimal change. The shear strength, cohesion (c), and internal friction angle (φ) of rockfill exhibit an exponential relationship with N. With the progression of cycles, the rate of particle breakage (B_r) and the increment in particle count diminish. **(2) Microscopic mechanism:** As N increases, the dense chain regions, areas of particle breakage, fracture distribution, and displacement field within the sample all expand overall, while the average coordination number rises significantly. However, beyond a certain N, these microscopic changes become less pronounced. **(3) Damage evolution:** The parameters A, B, and C of the modified Duncan-Chang model follow an exponential relationship with N. As N increases, these parameters exhibit exponential growth, with a marked increase during the early cycles, which stabilizes in the later cycles.

Keywords: Dry-wet cycle. Rockfill. Discrete element method. Mechanical properties. micrscopic mechanism

1 Introduction

Rockfill materials are commonly used in the construction of high rockfill dams due to their widespread availability, ease of handling, high bearing capacity, and favorable water permeability [1-3]. However, during the dam's operation, rockfill materials in areas subject to water level fluctuations are impacted by factors such as rainfall, evaporation, and

seasonal changes in reservoir levels. Repeated dry-wet cycles lead to the degradation of rockfill performance [4-6], which is evident in the reduction of shear strength and deformation modulus. This degradation can cause engineering issues like uneven deformation and slope instability in rockfill dams [7-11]. Hence,it is of great scientific significance and engineering value to systematically analyze the deterioration evolution mechanism and deformation response characteristics of rockfill materials during dry-wet cycles to ensure the structural safety and stable operation of high rockfill dams during long-term service.

Currently, research on the evolution of rockfill mechanical properties under dry-wet cycles remains limited. Existing studies primarily focus on the following aspects: **(1) Macroscopic physical experiments:** The academic community has carried out extensive and in-depth research on degradation mechanisms affecting rockfill integrity, , and obtained rich data through extensive laboratory experimentation and field tests [12-16]. (1) Regarding the deformation and strength of rockfill under dry-wet cycles, some experimental findings indicate that shear strength declines under these conditions [17], and failure strength decreases exponentially [18]. However, the underlying deterioration mechanism remains unclear. (2) Concerning particle breakage of rockfill under dry-wet cycles, studies show that the mineral composition and microstructure of rockfill particles undergo changes during repeated wet-dry cycles. Post-cycles, the particle breakage strength diminishes, and the extent of breakage increases, leading to a deterioration in the macroscopic mechanical properties of rockfill [19]. As wetting-drying cycles progress, both the peak stress of rockfill particles and the mean particle crushing strength decrease [20]. While the deformation and strength of rockfill materials under dry-wet cycles are closely related to particle breakage, current testing methods and technologies do not allow for real-time dynamic monitoring of the micrstructural evolution within rockfill particles. The discrete element method (DEM), proposed by Cundall et al. [21], is an auxiliary simulation technique widely used in laboratory tests. In recent years, DEM has gained significant traction in geotechnical engineering studies, particularly for investigating micrmechanisms, and has become a key area of focus for many researchers globally [22, 23]. **(2) micr-scale numerical simulations:** DEM simulations have been employed to quantitatively analyze the deterioration of rockfill materials subjected to multi-path environmental loading conditions. However, there remains a gap in research addressing the degradation characteristics of rockfill materials under dry-wet cycles from the perspective of particle breakage. (1) Single wetting: Certain studies have modeled single wetting of rockfill materials by adjusting the shear modulus and friction coefficient of particles [24]. Other researchers have developed generalized wetting models considering moisture's impact on particle friction coefficients and the degradation of particle strength [25], but the above models did not include the particle breakage factor into the research category of wetting deformation. Yang et al. [26] incorporated wetting effects by reducing particle shear modulus, friction coefficient, and intergranular bond strength, while also considering particle breakage in their numerical model. (2) Dry and wet creep: Zhao et al. [27] carried out numerical

simulation on the aging deformation characteristics of rockfill materials under dry-wet cycle conditions, analyzing various stress erosion and wetting modes to explore their creep and weathering mechanisms. (3) Dry-wet cycles: Wang et al. [28] employed FDM-DEM joint simulation to clarify the cross-scale transfer mechanism of rockfill system and revealed the macroscopic deformation of the rockfill under hydraulic cyclic loading, but their study did not address particle breakage. In conclusion, there remains a lack of systematic research on the macroscopic mechanical properties and microscopic deterioration mechanisms of rockfill materials under dry-wet cycles, particularly from the perspective of particle breakage.

Building on this, this study established a three-axis numerical model of large rockfill materials using DEM, selected appropriate macro-micr parameters, and conducted three-axis numerical simulations of rockfill materials subjected to varying dry-wet cycle times *via* a generalized dry-wet cycle model. The deformation, strength, and particle breakage of rockfill materials were analyzed from a macroscopic perspective, and the functional relationship between the number of dry-wet cycles and damage evolution was discussed. The research further investigated how the number of dry-wet cycles influences the deterioration and deformation mechanisms of rockfill from a microscopic viewpoint, considering force chain distribution, particle breakage distribution, crack distribution, displacement fields, and average coordination numbers. These findings offer crucial theoretical underpinnings and practical implications for understanding the degradation mechanisms of rockfill dam materials subjected to cyclic dry-wet conditions.

2 Developing of a numerical model of rockfill materials

2.1 Characterizing the microscopic morphology of the rockfill body

2.1.1 Obtaining rockfill material surface profiles

The research focused on dam rockfill material with a density of 2.76 g/cm^3 and a maximum particle size of 60 mm. The lithology ranged from fresh to slightly weathered, featuring a homogenous particle size distribution and pronounced angularity. Using 3D laser scanning technology, surface point cloud data was collected for rockfill particles of diverse shapes and sizes. The collected data underwent a series of processing steps, including point cloud registration, triangulation mesh generation, and noise filtering, to produce optimized 3D models of individual rockfill particles. These refined models were then integrated into PFC3D 6.0 through command - line scripting, generating discrete 3D particle units and constructing a comprehensive particle database, as shown in Fig. 1. To more accurately simulate experimental conditions and particle morphological features in numerical analyses, four typical particle morphologies were carefully selected for in - depth investigation.

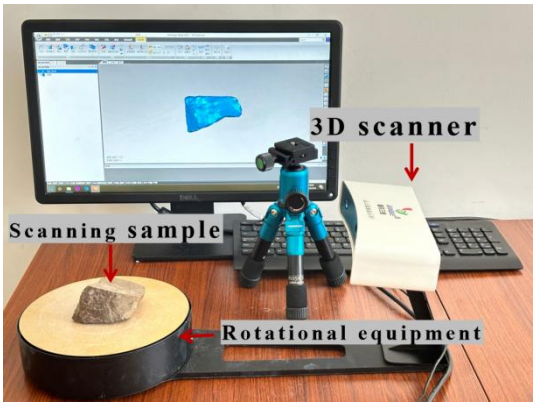
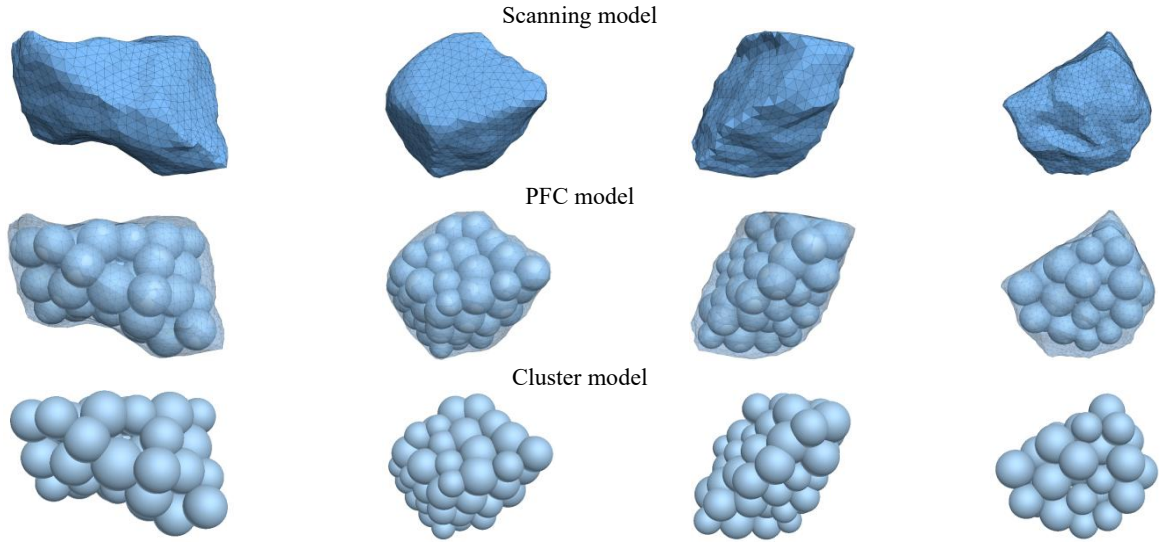


Fig.1 3D scanning device

2.1.2 Particle breakage characterization modeling

In order to construct a single particle numerical model, this study established a computational framework that can simulate the particle breakage process. The model is based on the geometry of the block stone obtained by three-dimensional scanning, and the method simulates the particle shape. Four typical rock samples were selected to generate cluster particle systems, and the parallel bond model was used to characterize the internal contact of particles. When the stress level at the bonding interface breaks through the strength limit of the material, it will lead to bond fracture and induce microcrack propagation. The particle breakage behavior is induced by simulating the dry-wet cycle process, so as to reproduce the deterioration mechanism of geotechnical materials. The single-particle model is depicted in Fig. 2.



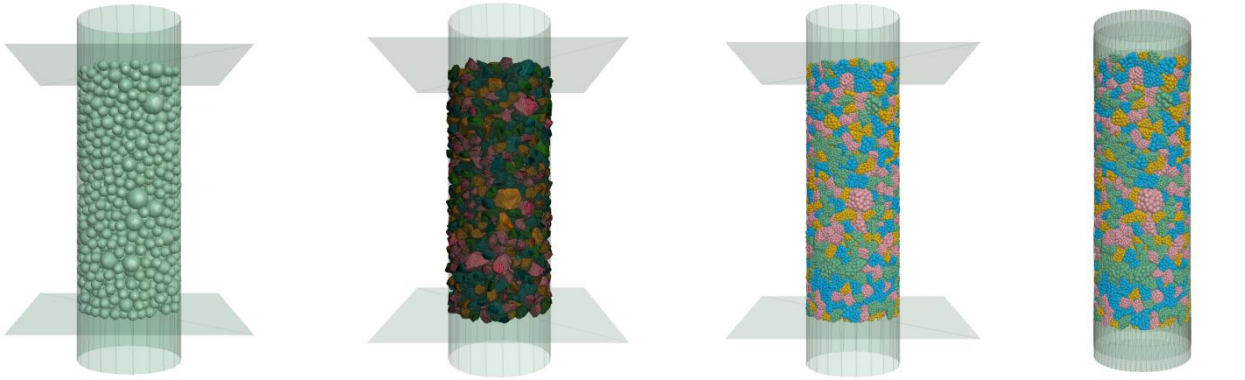
(a) Model 1 (b) Model 2 (c) Model 3 (d) Model 4

Fig.2 Single-particle model diagram

2.1.3 Preparing graded samples with deformable boundaries

The numerical model for rockfill material is constructed through the following procedure: First, an initial particle system is generated based on the target gradation. Subsequently, the assembly of loose spherical particles undergoes compression until reaching the preset dimensions (D×H: 300 mm×700 mm) and initial void ratio (e_0 = 0.93). During the compression and sample preparation stage, both the interparticle friction coefficient and gravitational acceleration are set to zero to suppress premature particle breakage. The basic spherical units are then replaced with clump

structures, which are further enhanced to a cluster particle system for simulation. Mechanical connections between clusters are established through a linear contact constitutive model (Fig. 3a-c). To establish the flexible boundary condition, a rigid boundary loading plate is first utilized to compact and densify the specimen. This is later switched to a PFC-FLAC coupled flexible boundary to accurately simulate the mechanical behavior of the latex membrane used in laboratory tests [29] (Fig. 3d). The final numerical model comprises 1,768 cluster units and 76,859 discrete particles.



(a) Samples are generated by grade (b) Particle clump replacement (c) Particle cluster replacement (d) Generation of flexible membranes

Fig.3 Sample model generation diagram

2.2 Generalized model of dry-wet cycle

Due to the presence of more cracks and defects in larger particles of rockfill, these cracks are more prone to expansion and breakage under external loads, which demonstrates the size effect phenomenon where particle breakage strength decreases as particle size increases. This phenomenon supports the idea that particle strength follows a Weibull distribution and is highly dependent on particle size [30]. The relationship between particle crushing strength σ_{f} and particle size d is as follows:

$$\sigma_{\mathrm{f}} = \left\{\ln\left[1/P_s(d)\right]\right\}^{1/m}\left(\frac{d}{d_0}\right)^{-(n_d/m)}\sigma_{\mathrm{m0R}} \tag{1}$$

In the formula, $P_{\mathrm{s}}(d)$ represents the survival probability of particles, m is the Weibull modulus, and the term n_{d}/m characterizes the size effect of particle crushing strength. σ_{m0R} is the unmodified characteristic crushing strength, d is the particle diameter, and d_0 is the characteristic particle diameter.

Compared to isolated single particles, particles within a system experience a "buffer effect" due to the constraints from surrounding particles, making them more resistant to breakage [31]. To quantify this effect, some experiments have investigated the impact of coordination number on breakage and proposed using the coordination number coefficient f_{CN} to correct the single-particle breakage strength [32]. Additionally, the curvature of the contact surface between particles influences the crushing strength. Thus, a curvature coefficient f_{d} is introduced for correction [33]. The modified relationship is as follows:

$$\sigma_{\mathrm{m0}} = \sigma_{\mathrm{Ru}} f_{\mathrm{CN}} f_{\mathrm{d}} \tag{2}$$

In the formula, σ_{Ru} represents the undeteriorated single-particle crushing strength; f_{CN} and f_d can be calculated using the following two equations:

$$f_{CN} = (CN-1)\exp\left[(\overline{D}/d)(CN-2)(CN-3)/4CN\right] \tag{3}$$

$$f_d = \frac{\overline{D}/d}{1+\overline{D}/d} \tag{4}$$

In the formula, CN is the coordination number of particles, and $\overline{D}$ is the average particle size of the surrounding particles.

The dry-wet cycle significantly deteriorates the mechanical properties of rockfill materials, but the single-particle crushing strength still follows the Weibull distribution. Moreover, σ_{Ru} is significantly influenced by the number of dry-wet cycles N [19]. The deterioration coefficient D_R is used to quantify the degree of particle deterioration and is defined as follows:

$$D_R = \sigma_{Rd}/\sigma_{Ru} \tag{5}$$

In the formula, σ_{Rd} represents the single-particle crushing strength after degradation. The single-particle crushing strength is determined based on the indoor single-particle crushing test results.

Based on the fitting analysis of single-particle breakage test results under different dry-wet cycles in Reference [19], as shown in Fig. 4, the deterioration coefficient D_R decreases exponentially with the increase of N, and the expression is as follows:

$$D_R = m + n\exp(lN) \tag{6}$$

In the formula, m, n, and l are the fitting parameters. By fitting the experimental data in reference [7], the values are obtained as follows: m = 0.667, n = 0.33, and l = -0.1414. Therefore, the characteristic crushing strength σ_{md} of the degraded particles is as follows:

$$\sigma_{md} = \sigma_{Ru} f_{CN} f_d D_R \tag{7}$$

By combining formula (7) and formula (1), the framework of the particle crushing strength model, which accounts for the effect of the dry-wet cycle, can be constructed.

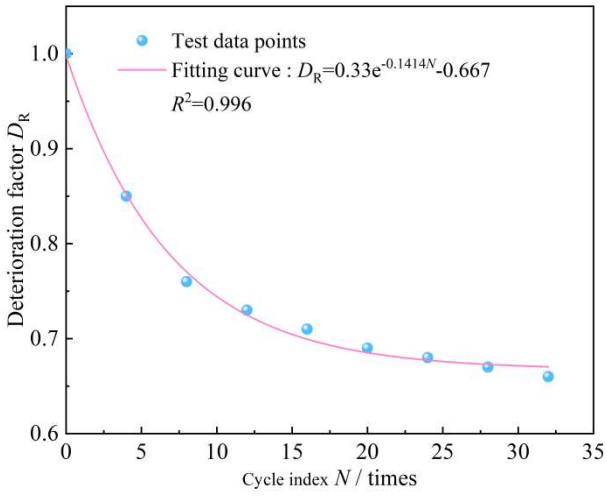


Fig.4 The relationship between Weibull distribution parameters and dry-wet cycle

During dry-wet cycles, the surface contact modulus, friction coefficient, and inter-particle bond strength within the rockfill particle numerical model are reduced. To simulate the deterioration of the particle breakage model under dry-wet cycles, the deterioration coefficient D_R is applied to scale down the surface contact modulus, friction coefficient, and inter-particle bond strength. The relationship is as follows [26, 27]:

$$E_{Rd}^{*} = E_{Ru}^{*} D_R \tag{8}$$

$$\mu_{Rd} = \mu_{Ru} D_R \tag{9}$$

$$\sigma_{Rd} = \sigma_{Ru} D_R \tag{10}$$

In the formula, E_{Ru}^{*} and E_{Rd}^{*} represent the contact modulus of the rockfill particle numerical model before and after surface deterioration, respectively; μ_{Rd} and μ_{Ru} are the friction coefficients before and after surface deterioration; σ_{Rd} and σ_{Ru} denote the bond strength between the particles before and after the deterioration of the numerical model of rockfill particles.

2.3 Selection of macro and micro parameters and model verification

2.3.1 Selection of contact model

In the previous chapters, the selection method of contact model has been discussed in depth. Aiming at the problem of particle breakage, this study regards cluster particles as deformable entities for simulation. Inside the cluster particles, the parallel bond model is used to construct, which can accurately describe the mechanical properties of broken rocks. In the numerical model, the interaction at the interface of the particle cluster and the flexible membrane is realized by a linear contact model, which only allows the membrane to transfer normal force and tangential force to the particle, excluding the transfer of torque. This treatment method can more realistically restore the mechanical response of the rubber film under flexible pressure in the indoor triaxial test.

2.3.2 Determination of macro parameters

When selecting macro- and micro-parameters, rationality and reliability should be given top priority, as the precision of these values significantly impacts the validity of numerical experiments. Given that existing parameter values cannot be obtained directly from experimental measurements, they are typically determined via iterative adjustment or by drawing analogies from similar studies. Based on the stress-strain characteristics obtained from triaxial compression tests of rockfill materials, Table 1 summarizes the key macroscopic material parameters. These parameters encompass the deformation modulus (E), Poisson's ratio (v), internal friction angle (φ), and peak shear strength (σ_{max}). These values correspond to the testing conditions of a 1200 kPa confining pressure.

Table 1 Macroscopic parameters

sample state	E/MPa	v	φ/°	σ_{max}/MPa
drying	212.546	0.385	39.5	5.827

2.3.3 DEM micro-parameter characterization and interparticle contact validation

At the beginning of the study, the micrscopic parameters of rockfill materials were preliminarily calibrated. Although the numerical simulation results presented by this parameter combination are highly consistent with the indoor test data, the rationality of the parameters still needs to be verified in depth. Therefore, in this study, the initial values of micrscopic parameters were optimized by response surface method, and the mapping relationship between micrscopic parameters and deviatoric stress of rockfill materials to be inverted was constructed [34]. The specific expressions are as follows:

$$s_k(\bar{x}) = a + \sum_{i=1}^{3} b_i \bar{x}_i^2 + \sum_{i=1}^{3} c_i \bar{x}_i^2 \tag{11}$$

$$\bar{x} = [\bar{x}_1, \bar{x}_2, \bar{x}_3]^T = [\bar{k}_n, \bar{k}_s, \bar{f}]^T \tag{12}$$

$$\bar{k}_n = \frac{k_n}{\tilde{k}_n}, \bar{k}_s = \frac{k_s}{\tilde{k}_s}, \bar{f} = \frac{f}{\tilde{f}} \tag{13}$$

In the formula, s_k enotes the deviatoric stress at the kth load increment; coefficients a, b_i, and c_i are unknown polynomial parameters; the vector $\bar{x}$ contains dimensionless independent variables; while $\bar{k}_n$, $\bar{k}_s$, and $\bar{f}$ represent the normalized normal contact stiffness, tangential contact stiffness, and friction coefficient, respectively; the micr-parameters $\tilde{k}_n$, $\tilde{k}_s$, and $\tilde{f}$ of rockfill material are determined based on empirical estimation method.

Based on the micrscopic parameters in Table 2, the numerical simulation of crushability triaxial compression is carried out. Fig.5 shows that the simulated stress-strain curve and the indoor test results show significant convergence characteristics, which effectively verifies the ability of the parameters to characterize the mechanical behavior of rockfill materials, and further confirms the rationality and reliability of the parameter system in Table 2.

Table 2 Numerical simulation of micrscopic parameters

	mechanical parameter	drying
linear	lnm_krat	1.5
	lnm_emod/Pa	10×10^9
	lnm_fric	0.3
linearpbond	pbm_emod/Pa	2.5×10^9
	pbm_ten/Pa	3.5×10^7
	pbm_coh/Pa	2.333×10^7
	pbm_fa/°	50
	pbm_kn/Pa	10×10^9
	pbm_ks/Pa	2.5×10^9
	pbm_fric	0.2

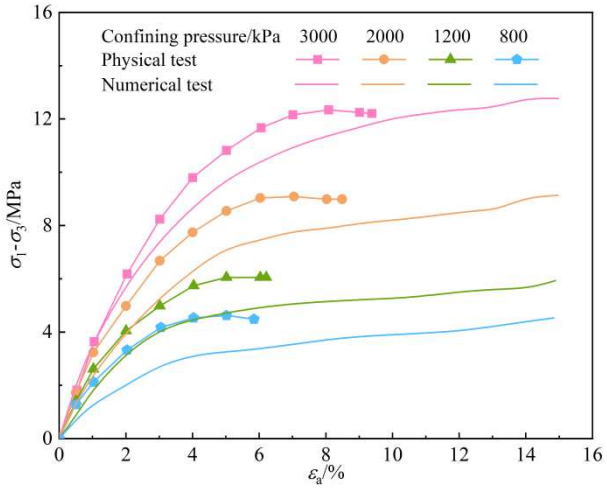


Fig.5 Comparison diagram of the numerical test and the physical test results

2.4 Test scheme

In the present investigation, numerical simulation tests were carried out for 4 distinct groups of confining pressures and 5 sets of dry-wet cycles, as outlined in Table 3. When the specimen reaches the peak shear strength or the axial strain is 15 % ~ 16 %, the loading process is terminated to test the relationship between the deformation and the stress state of the rockfill.

Table 3 Test scheme

cycle index *N* / times	confining pressure / kPa
0	800、1200、2000、3000
8	800、1200、2000、3000
16	800、1200、2000、3000
24	800、1200、2000、3000
32	800、1200、2000、3000

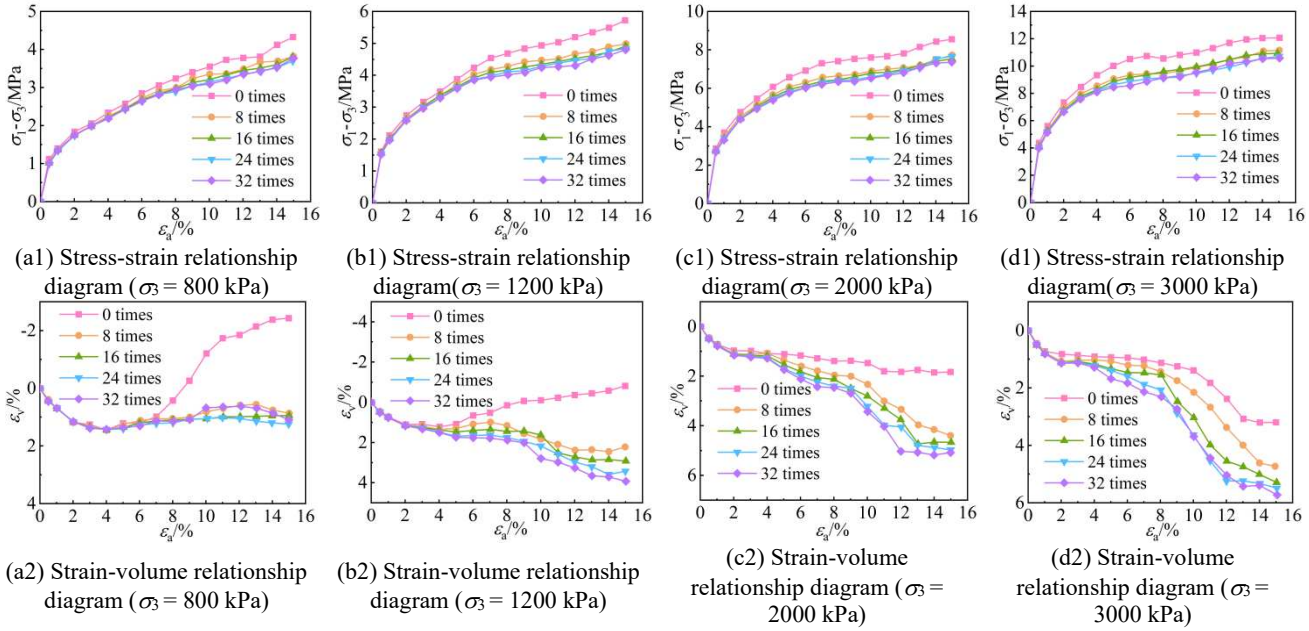
3 Experimental results and analysis

3.1 Macroscopic results analysis

3.1.1 Test deformation analysis

Fig. 6 presents the deformation relationship curve for the rockfill dry-wet cycle test. As seen in Fig. 6(a), the dry-wet cycle induces a strain-hardening deviatoric stress-strain curve for the rockfill. As *N* increases, the tangent modulus and peak stress decrease nonlinearly. Beyond a certain value of *N*, the decline becomes more gradual, and the deteriorating performance stabilizes. Fig. 6(b) shows that under confining pressures of 800 kPa and 1200 kPa, the rockfill material initially exhibits shear shrinkage during the early stages of loading, transitioning to dilatancy as the axial strain increases. Under other confining pressures, shear shrinkage is still observed. However, after several dry-wet cycles, the material initially shears and then expands under 800 kPa confinement, though the shear expansion is notably smaller than in the non-cycled case. Obvious shear contraction is consistently observed under other confining pressures. Additionally, the dry-wet cycle inhibits volume deformation, including both shear contraction at the initial loading stage

and dilatancy at later stages. However, as N increases, this inhibition effect weakens. Overall, the negative impact of dry-wet cycles on the mechanical properties of rockfill materials has an upper limit, and the deterioration process does not continue indefinitely with cycle accumulation.



(a1) Stress-strain relationship diagram (σ_3 = 800 kPa)
(b1) Stress-strain relationship diagram(σ_3 = 1200 kPa)
(c1) Stress-strain relationship diagram(σ_3 = 2000 kPa)
(d1) Stress-strain relationship diagram(σ_3 = 3000 kPa)

(a2) Strain-volume relationship diagram (σ_3 = 800 kPa)
(b2) Strain-volume relationship diagram (σ_3 = 1200 kPa)
(c2) Strain-volume relationship diagram (σ_3 = 2000 kPa)
(d2) Strain-volume relationship diagram (σ_3 = 3000 kPa)

Fig.6 The deformation relationship curve of rockfill dry-wet cycle test

3.1.2 Test strength analysis

Fig. 7 illustrates the strength relationship curve of rockfill dry-wet cycle test. As shown in Fig. 7, dry-wet cycle progressively compromisesthe peak strength of rockfill. Due to the effect of dry-wet cycles, physical and chemical changes occur inside the rockfill, resulting in material degradation, which in turn leads to a significant reduction in strength and peak stress attenuation. The peak strength difference between 0 and 8 cycles is more significant, while the difference between 16, 24, and 32 cycles becomes smaller. This is because the rockfill material does not degrade indefinitely during dry-wet cycles. As shown in Fig. 7, the peak strength σ_{max} and the number of dry-wet cycles N correlation is well-described by linear fitting, expressed as follows:

$$\sigma_{max} = ae^{bN} + d \tag{14}$$

In the formula, σ_{max} represents the peak strength, a, b, and d are the fitting parameters, and N is the number of dry-wet cycles.

The fitting results demonstrate a negative correlation between the sample's failure strength and the number of dry-wet cycles N, indicating a progressive decline in strength as N increases. The damage effect from the dry-wet cycle diminishes with the rise in N. Once N reaches a critical value, the propagation of micro-cracks within the particle reaches its upper limit, and the cumulative damage stabilizes, entering a steady stage.

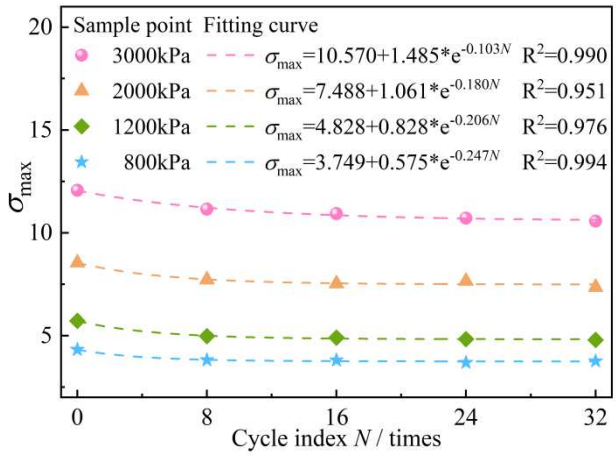


Fig.7 The strength relationship curve of rockfill dry-wet cycle test

Fig. 8 illustrates the relationship between the number of dry-wet cycles and c, φ (3000 kPa). As shown in Fig. 8, an increase in the number of dry-wet cycles N leads to the deterioration of the internal structure of the sample, weakening the intergranular forces and reducing the cohesion. Simultaneously, particle breakage is exacerbated, resulting in a decrease in peak strength as the number of cycles increases. The cohesion c and the number of dry-wet cycles N can be fitted by a linear function, expressed as follows:

$$c = fe^{gN} + h \tag{15}$$

In the formula, c represents the cohesive force, f, g, and h are the fitting parameters, and N is the number of dry-wet cycles.

The internal friction angle φ reflects the frictional resistance characteristics of the soil, which includes the sliding friction μ_1 caused by the relative slip between particles and the bite friction μ_2 resulting from the detachment state. The internal friction angle φ is positively correlated with the frictional resistance μ.

$$\mu = \mu_1 + \mu_2 \tag{16}$$

In the formula, μ represents the total frictional resistance, μ_1 is the sliding friction, and μ_2 is the occlusal friction.

Fig. 8 illustrates the relationship between the number of dry-wet cycles and c, φ (3000 kPa). As shown in Fig. 8, peak stress decreases with an increasing number of dry-wet cycles N. The dry-wet cycle progressively damages the internal structure of the sample, leading to gradual deterioration. This results in the simultaneous weakening of both sliding friction μ_1 and occlusal friction μ_2 during the slip dislocation process, causing a decrease in the total frictional resistance μ. The initial internal friction angle φ drops from 39.63° to 37.57°, reflecting a reduction of 5.20%. As depicted in Fig. 8, the internal friction angle φ exhibits a linear relationship with the number of dry-wet cycles N, as follows:

$$\varphi = ie^{jN} + k \tag{17}$$

In the formula, φ represents the internal friction angle, i, j, and k are the fitting parameters, and N is the number of dry-wet cycles.

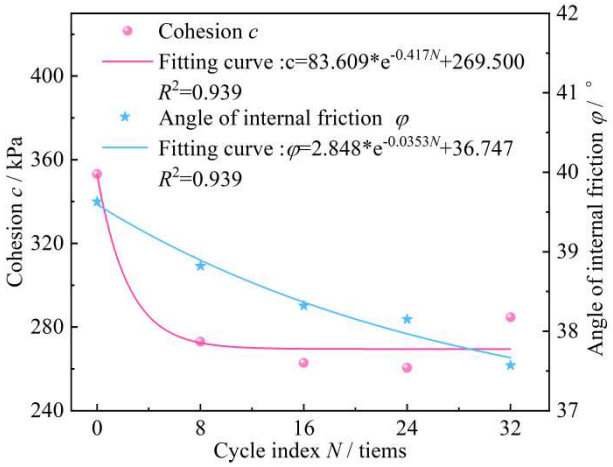


Fig.8 The relationship between the number of dry-wet cycles and c, φ (3000 kPa)

3.1.3 Test particle breakage analysis

3.1.3.1 Grain breakage

Particle breakage is a primary factor driving the deterioration and deformation of rockfill materials, and its quantitative analysis requires selecting indicators that precisely capture the extent of breakage. Current quantitative methods can be broadly categorized into two approaches: single-particle scale analysis and statistical measurements of particle groups. These methods are primarily suited for physical experiments. In DEM simulations,the number of bond fractures is often used as a characterization index of the breakage rate [35], and its expression is :

$$B_r = n / N_1 \tag{18}$$

In the formula, n represents the number of broken links, and N_1 denotes the total number of links.

Fig. 9 presents the relationship between B_r and vertical strain during the dry-wet cycle test. As observed in Fig. 9, that the particle breakage rate (B_r) shows a significant correlation with the vertical strain. It is found that when the vertical strain exceeds the 4 % threshold, the particle breakage rate shows a sharp growth trend. It is worth noting that the effect of different cycles on the increment of particle breakage rate is significantly different, which indicates that the Br-strain relationship is simultaneously regulated by the number of cycles and confining pressure. In the early cycles, the B_r increment is notably larger, and as the number of cycles increases, this increment diminishes substantially. At a given number of cycles, B_r exhibits an upward trend as the confining pressure increases. The analysis suggests that while the influence of confining stress on the deteriorating behavior of rockfill particles breakage rate is smaller compared to the number of cycles, particle breakage in rockfill materials is more pronounced during the initial cycles, with a smaller increase in the later cycles. This is primarily due to that the rockfill material deteriorates during the dry-wet cycles but does not degrade indefinitely. In the early stages of cycling, smaller particles fill the pores, which limits the flipping and movement of the rockfill sample in subsequent cycles. This results in a more gradual rise of B_r during subsequent cycles.

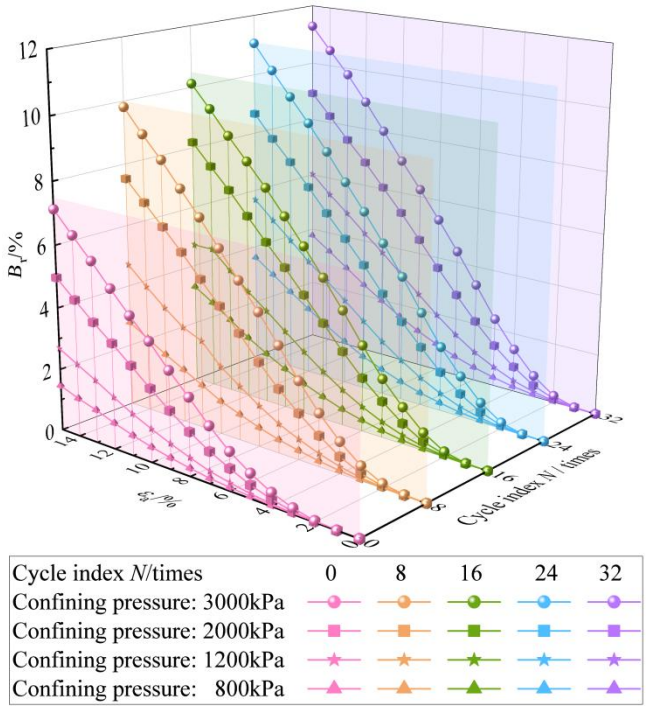


Fig.9 The relationship between B_r and vertical strain in dry-wet cycle test

3.1.3.2 Particle count

Fig. 10 presents the relationship between particle count and vertical strain in dry-wet cycle test. As shown in Fig. 10, when the strain exceeds 6%, the number of particles increases significantly. At low stress levels, this increase is mainly due to small strains caused by elastic compression and interparticle slip mechanisms. At high stress levels, it results primarily from large deformations caused by particle breakage. During the early cycles, particle breakage is prominent, thereby substantially elevating fragmentthe number of new particles. In later cycles, particle breakage becomes less pronounced, and the number of new particles increases at a slower rate. This analysis indicates that the number of particles increases due to both the water-induced deterioration of rockfill and the particle breakage caused by dry-wet cycles. However, the degree of deterioration does not continue to escalate indefinitely with the number of cycles, which aligns with the observed trend in the particle breakage rate.

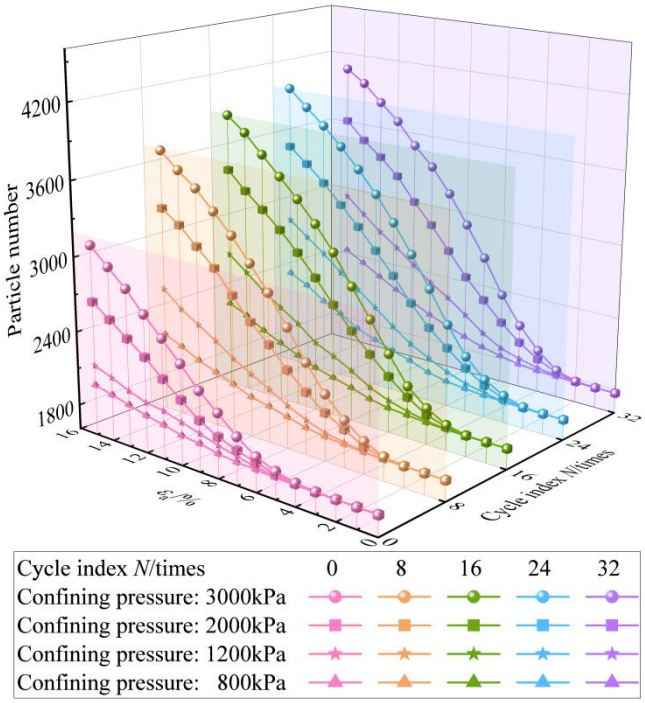


Fig.10 The relationship between particle count and vertical strain in dry-wet cycle test

3.1.3.3 Unified relationship of rockfill particle breakage

Previous test results demonstrate that the particle breakage rate of rockfill is closely linked to the number of dry-wet cycles *N*. When the same initial sample is loaded to an equal strain, the corresponding breakage rates for different values of *N* vary significantly. The relationship between *N* and the breakage rate, based on conventional tests, fails to reflect the actual complex load conditions. With increasing *N*, the evolution of particle size distribution follows a consistent pattern, suggesting a unified crushing evolution mechanism for rockfill materials.

According to previous studies [36-38], the occurrence of particle breakage is an energy-consuming process, and a relationship between input energy and particle breakage has been established. The external work W (total input energy) in the shear process of the sample is composed of elastic work W_e and plastic work W_p. The relationship is as follows:

$$\begin{cases} \Delta W = \Delta W_e + \Delta W_p \\ \Delta W_e = \left[(\sigma_1 - \sigma_3)\Delta\varepsilon_1^e + \sigma_3\Delta\varepsilon_v^e\right] \\ \Delta W_p = \left[(\sigma_1 - \sigma_3)\Delta\varepsilon_1^p + \sigma_3\Delta\varepsilon_v^p\right] \end{cases} \tag{19}$$

In the formula: $\Delta\varepsilon_1^e$ represents the elastic axial strain increment; $\Delta\varepsilon_v^e$ denotes the elastic volume strain increment; $\Delta\varepsilon_1^p$ is the plastic axial strain increment; $\Delta\varepsilon_v^p$ is the plastic volumetric strain increment; σ_1 is the major principal stress; and σ_3 is the minor principal stress.

The commonly used formula for calculating plastic work is shown in (20):

$$W_p = \int p'\left\langle \mathrm{d}\varepsilon_v^p \right\rangle + q\mathrm{d}\varepsilon_1^p \tag{20}$$

In the formula, p represents the average principal stress; q denotes the deviatoric stress; $\Delta\varepsilon_v^p$ is the plastic volumetric strain; and $\Delta\varepsilon_1^p$ is the plastic shear strain.

The total energy change during the triaxial shear process can be approximated by the change in plastic work W_p. The relationship is as follows [39]:

$$W_p \approx \int \mathrm{d}W = \int \sigma_3 \mathrm{d}\varepsilon_v + \int (\sigma_1 - \sigma_3)\mathrm{d}\varepsilon_1 \tag{21}$$

In the formula, the plastic work is the sum of the area enclosed by the principal stress difference σ_1-σ_3 and the axial strain $\mathrm{d}\varepsilon_1$, the confining pressure σ_3, and the volume strain curve during the triaxial shear test.

Fig. 11 illustrates the relationship between B_r and W_p for rockfill under different dry-wet cycles. As presented in Fig. 11, The data demonstrate a consistent positive correlation: B_r systematically increases with W_p across all cycle counts, exhibiting limited data scatter. Notably, higher cycle numbers amplify B_r values at equivalent W_p levels. The relationship is as follows [40]:

$$B_r = W_p / (l + mW_p) \tag{22}$$

In the formula, l and m are material parameters.

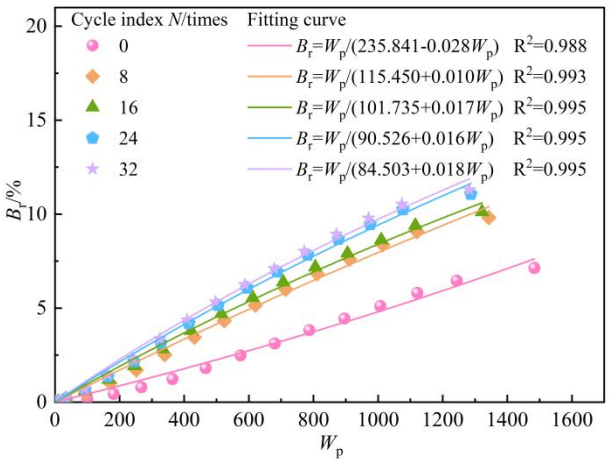


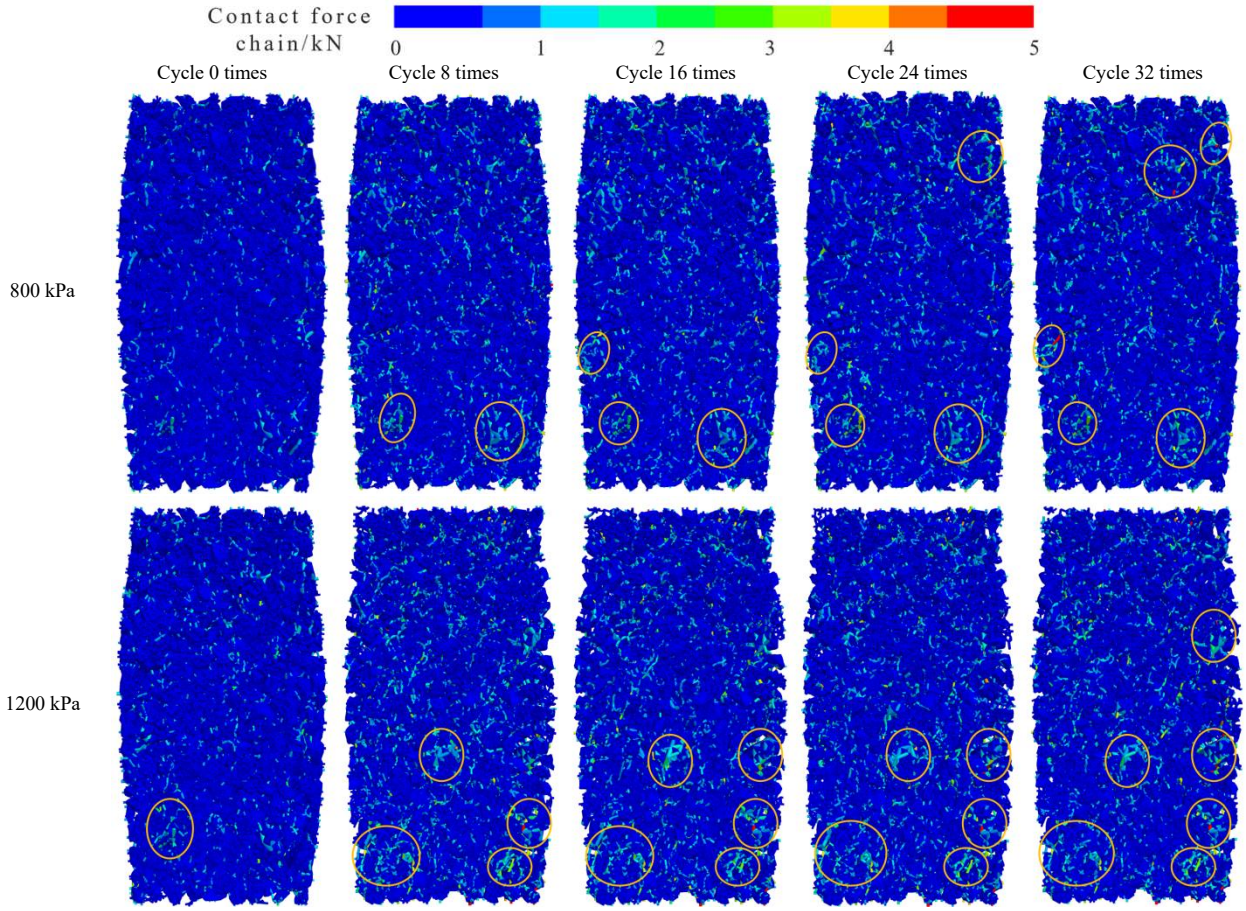
Fig.11 The relationship between B_r and W_p of rockfill under different cycles

3.2 Analysis of microscopic results

Research on the mechanical mechanisms of rockfill materials and the establishment of a macro-micr cross-scale correlation has gained widespread recognition and is highly valued by scholars both domestically and internationally from a microscopic perspective. By leveraging the capabilities of the DEM to "visualize" the mechanical behavior of rockfill materials under dry-wet cycles at the micr-scale, the evolution of its internal micr-mechanisms is quantitatively analyzed, ultimately establishing the physical relationship between these micr-mechanisms and the deterioration of macro-mechanical properties.

3.2.1 Contact force chain distribution

Fig. 12 presents the distribution map of contact force chain of filling soil in dry-wet cycle test. As shown in Fig. 12, when the confining pressure escalates incrementally from 800 kPa to 3000 kPa, the density of the strong contact force chain exhibits a pronounced positive strengthening tendency. The old strong contact force chains around broken particles are more noticeably lost, while new strong contact force chains form. The density of the strong contact force chain increases with the number of cycles, but the increment becomes small once the cycle number reaches a certain threshold. The locations of particle breakage correspond closely to the distribution of strong contact force chains. The breakage mechanism is attributed to the peak contact forces sustained by the particles. At 3000 kPa confining pressure, strong contact force chain density intensifies substantially compared to 800 kPa conditions. This densification induces macroscopic sample stiffening and elevates deviatoric stress.



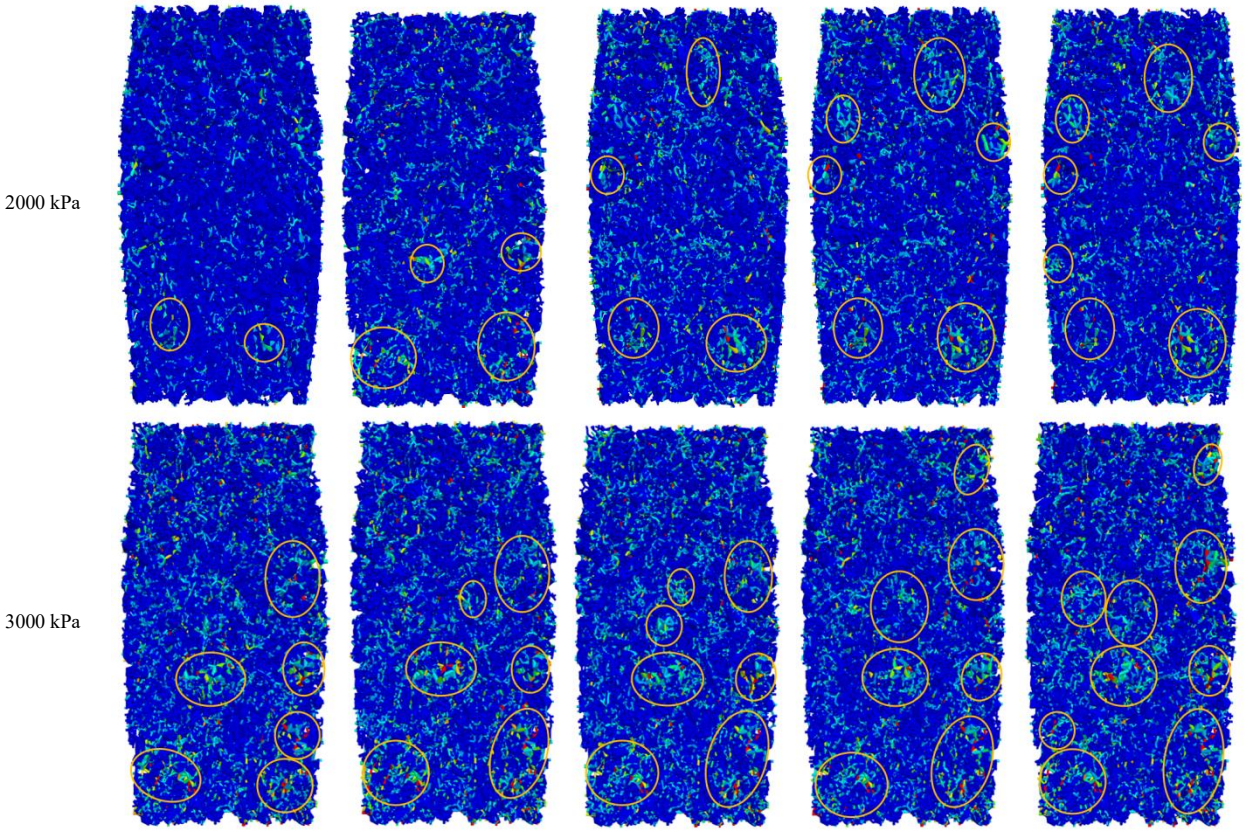
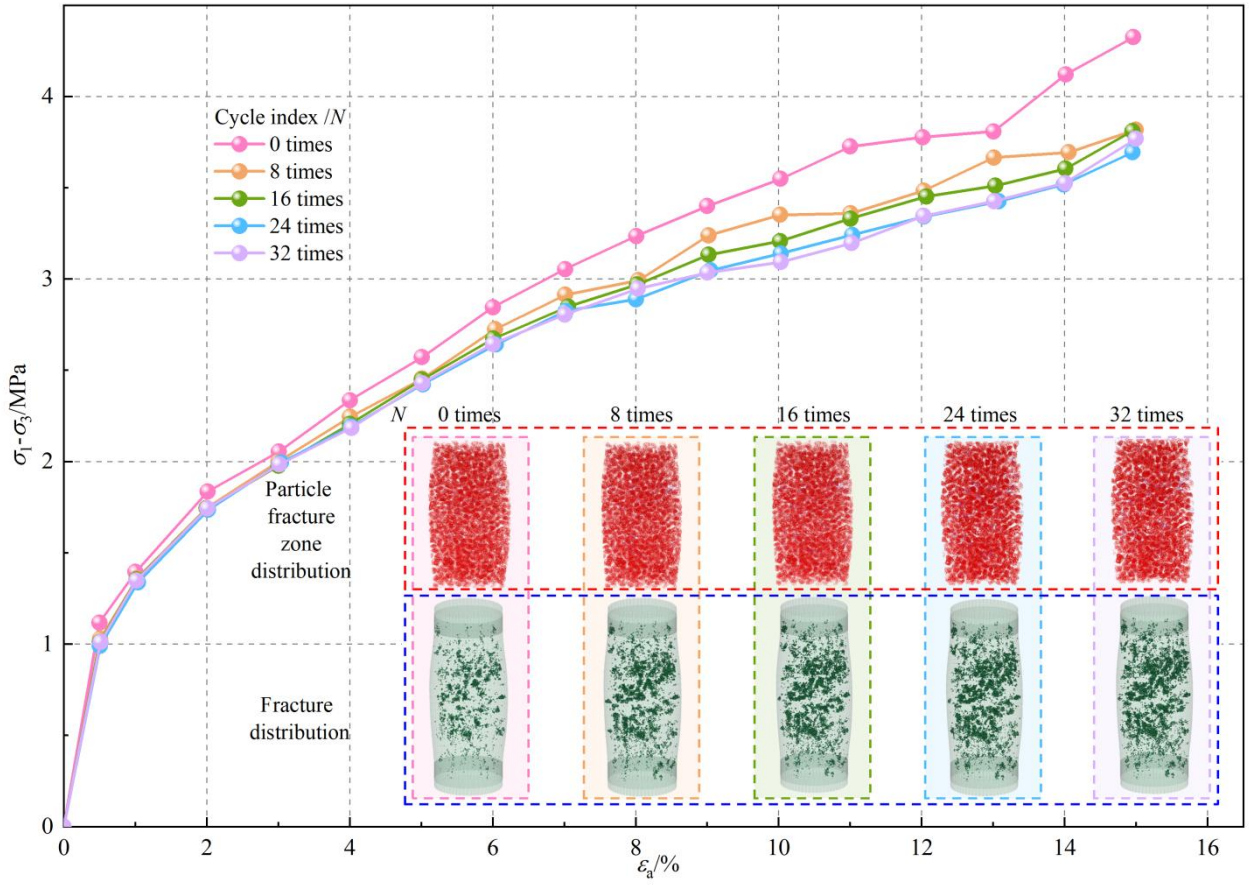


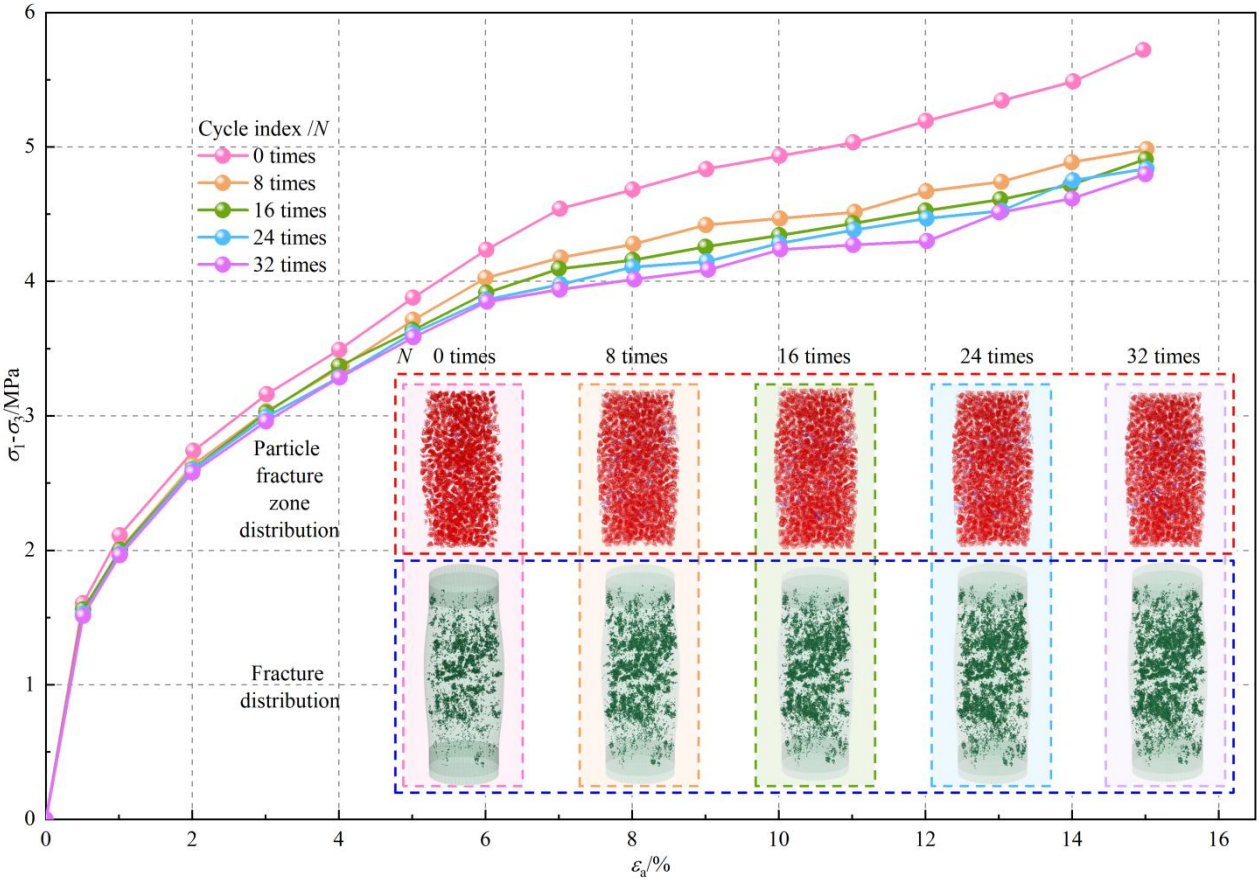
Fig.12 Distribution map of contact force chain of filling soil in dry-wet cycle test

3.2.2 Particle breakage distribution

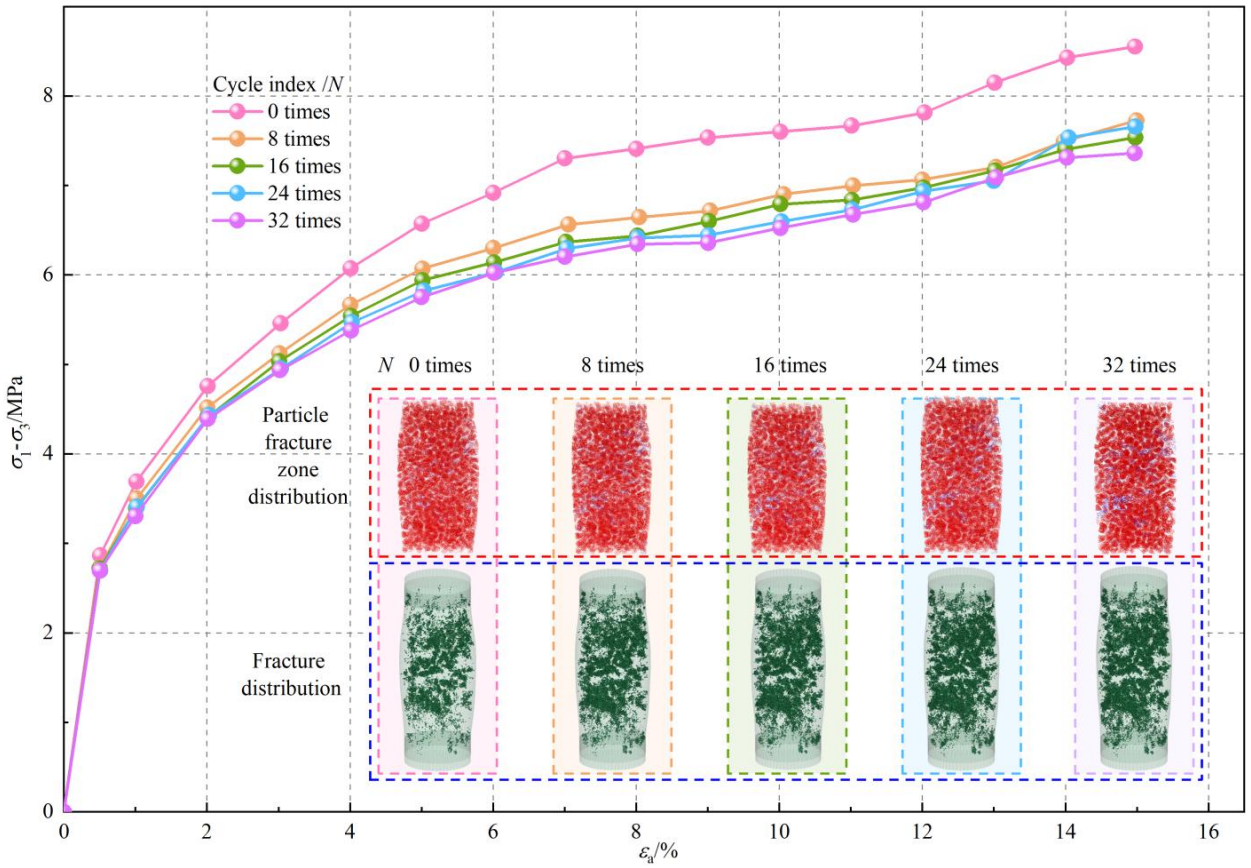
Fig. 13 presents The distribution of particle breakage position and fracture position of filling soil in dry-wet cycle test. As shown in Fig. 13, the extent of particle breakage is influenced by two main factors. First, both the range of particle breakage and fracture distribution expand with increasing confining pressure. Second, the extent also significantly increases with the number of dry-wet cycles *N*; however, once *N* reaches a certain threshold, the growth rate slows. The spatial distribution of particle breakage reveals that broken particles tend to concentrate along the diagonal, with localized clusters. This localized concentration effect intensifies as *N* increases. The underlying mechanisms are as follows: (1) Dynamic mechanical redistribution: Particle slip and rotation lead to recombination of the contact force chain, while local extrusion and collisions cause a sharp increase in contact force (as shown in Fig. 12, illustrating force chain evolution); (2) Cascading fracture effect due to strength deterioration: The development of cracks reduces the particle strength, and localized capacity attenuation under external loads triggers cascading fractures (Fig. 13).



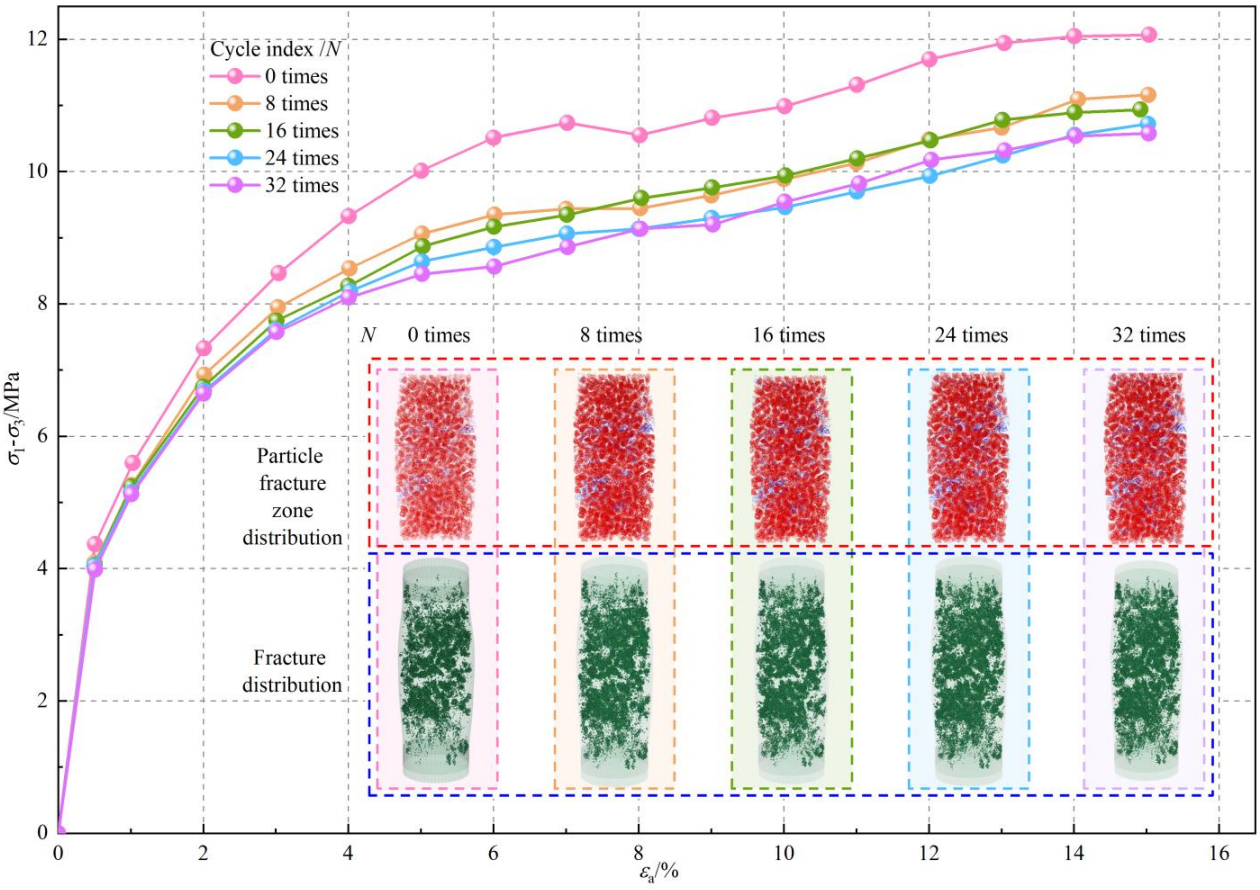
(a)σ_3=800 kPa



(b)σ_3=1200 kPa



(c)σ_3=2000 kPa

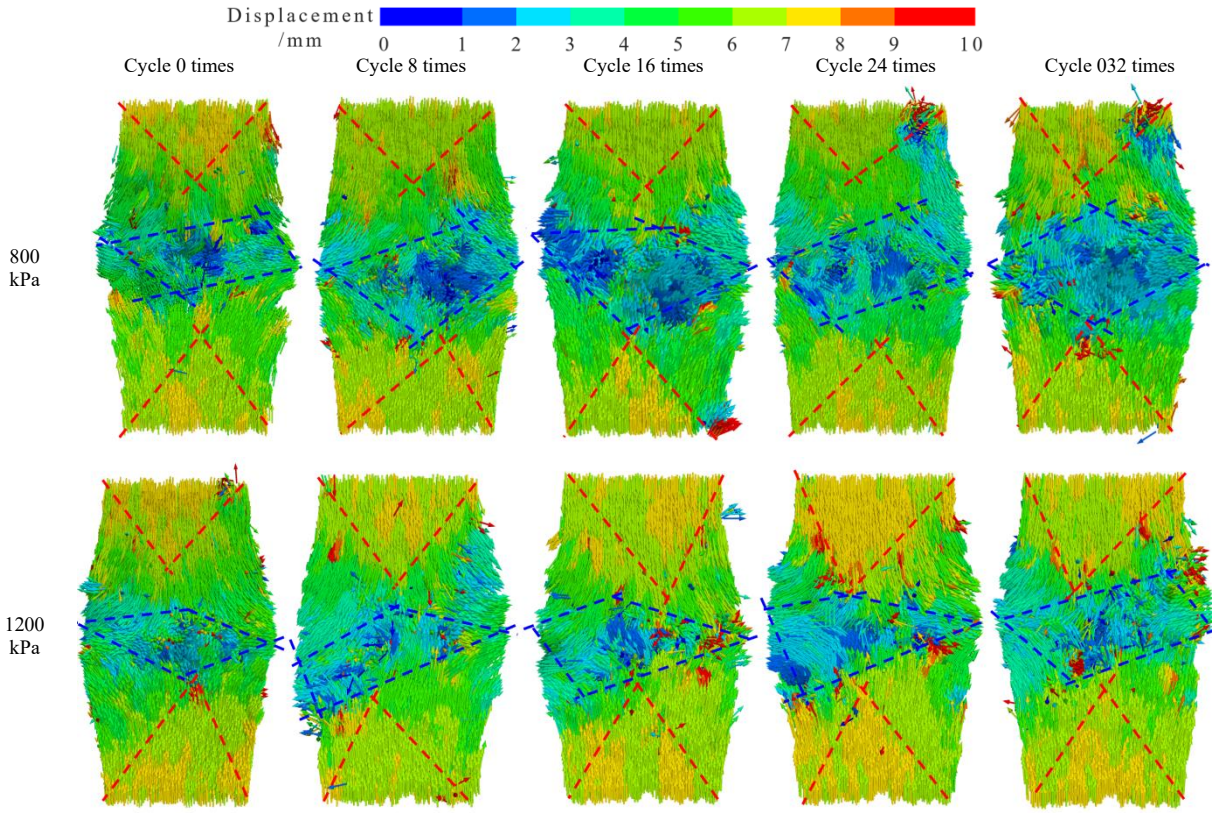


(d)σ_3=3000 kPa

Fig.13 Distribution of particle breakage position and fracture position of filling soil in dry-wet cycle test

3.2.3 Displacement field

Fig. 14 presents the displacement distribution of filling particles in dry-wet cycle test. In the study of particle motion state and sample bulging failure process, we accurately mark the particle motion trajectory through the streamline with arrows, and visually present its dynamic change trend. The gradient chromatographic system from blue to red is used to quantify the displacement parameters. The cold tone blue represents a small displacement, and the displacement increases step by step as the color transitions to warm tone red.The central blue area corresponds to the sample's bulging region, serving as a direct indicator of dilatancy magnitude. As depicted in Fig. 14, this damage zone exhibits distinct dynamic evolution - its spatial extent demonstrates continuous enlargement under cyclic loading. The essential reason for this phenomenon is that the periodic action of cyclic load promotes the complex mechanical response of particles. With the accumulation of the number of cycles, the interaction strength between particles is increasing, and the original stable stacking structure is gradually destabilized. In this process, the particle turnover behavior becomes more frequent, and some particles are broken under repeated stress. The combined effect of the two causes the continuous expansion of the bulging failure area.



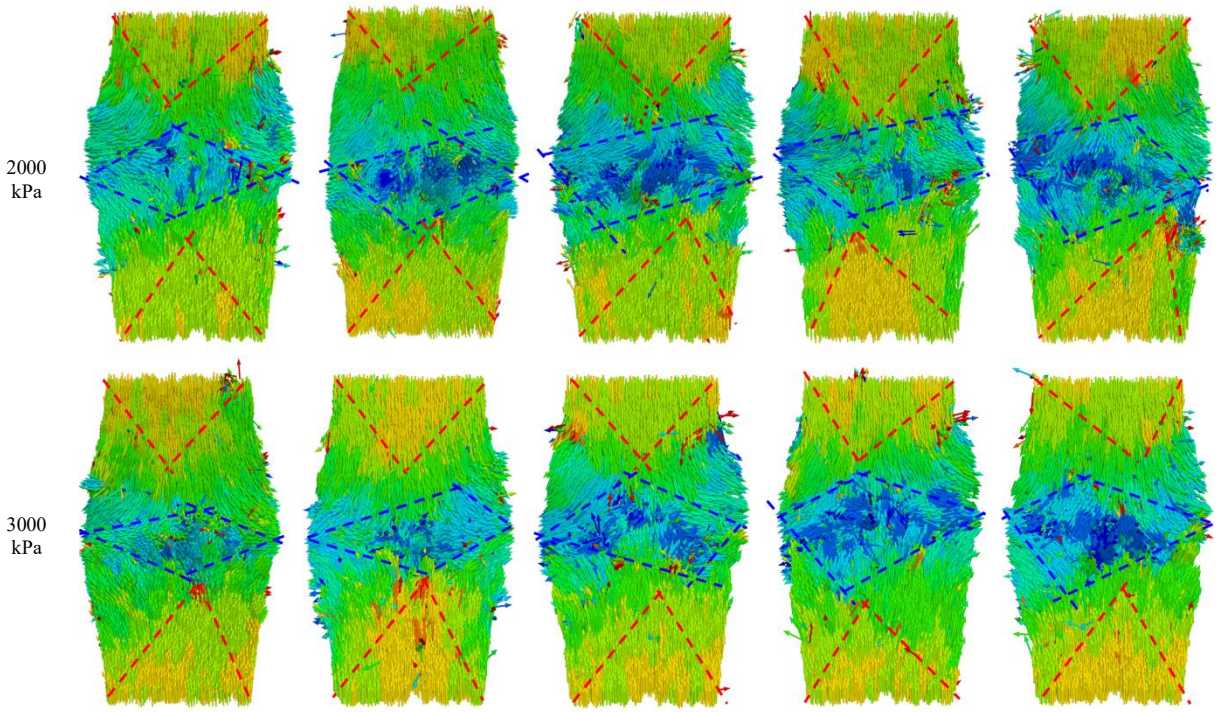


Fig.14 Displacement distribution of filling particles in dry-wet cycle test

3.2.4 Mean coordination number

As the core index in the micr-mechanical analysis of rockfill materials, the average coordination number refers to the average contact number of unit particles with other particles in the space system. By quantifying the topological connection between particles, this parameter can accurately describe the structural stability characteristics inside rockfill materials. When the average coordination number is high, it means that the particle system forms a closer interlocking network, showing stronger shear and deformation resistance under load. On the contrary, the lower average coordination number implies that the structure is loose, and the particles are prone to relative sliding and flipping, which may lead to system instability. Therefore, the average coordination number not only directly reflects the contact tightness between particles, but also is an important theoretical basis for predicting the mechanical behavior of rockfill materials under different working conditions. It has important application value in engineering fields such as dam stability analysis and foundation treatment.

The average coordination number C_a can be expressed as follows [41]:

$$C_a = \frac{2N_c}{N_p} \tag{23}$$

In the formula, N_c is the total number of contacts in the sample; N_p is the number of particles in the sample.

Fig. 15 illustrates the spatial distribution of coordination numbers during the shear process of samples that have undergone 32 dry-wet cycles under a confining pressure of 2000 kPa. As shown in Fig. 15, the coordination number decreases overall during the shearing process, with the variation patterns in the upper and lower sections being largely similar. The reduction in the coordination number at the center is more pronounced compared to the upper and lower

parts. Experimental results also reveal significant particle movement in the center of the sample, which aligns with the formation of the shear band.

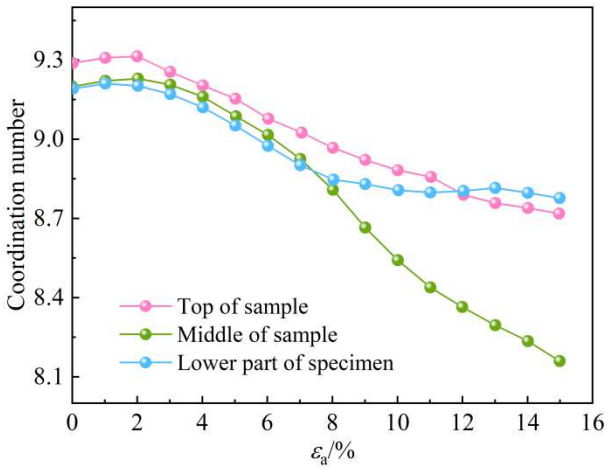


Fig.15 Evolution of coordination number in different positions of dry and wet cycle samples (2000 kPa, $N = 32$)

Fig. 16 presents the evolution curve of the average coordination number for rockfill under dry-wet cycle testing at various confining pressures. As presented in Fig. 16, the phase lag phenomenon is evident: due to particle breakage, the peak of the average coordination number curve lags behind the phase transition point of the volume strain. Additionally, monotonic growth characteristics are observed: the average coordination number continuously increases with the number of dry-wet cycles N. In the early stages, the difference in the average coordination number is significant, while in the later stages, the increase in this difference becomes less pronounced.

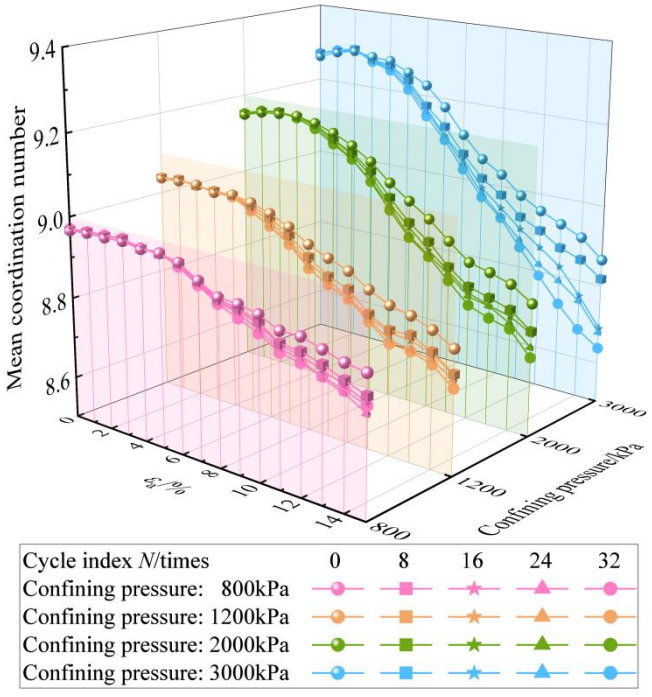


Fig.16 Evolution curve of average coordination number under dry and wet cycles with different rockfill compaction pressures

4 Damage evolution of mechanical properties of rockfill materials

4.1 Improved Duncan-Chang nonlinear model

A limitation of the Duncan-Chang model is its inability to accurately fit the partial dilatancy stress-strain curve and the volumetric strain curve [42]. To address this, our research group enhanced the Duncan-Chang model [43] and verified its performance. The results indicate that the improved model offers a good overall fit, effectively resolving the issue of the traditional nonlinear model's inability to fully capture the softening curve, thereby improving its predictive accuracy.

In the improved Duncan-Chang model, the stress-strain relationship formula is as follows [43]:

$$\sigma_1 - \sigma_3 = \frac{\varepsilon_1}{A + B\varepsilon_1 + C\varepsilon_1^2} \tag{24}$$

In the formula: A, B, and C are model parameters.

The differential solution of E_t (24) is performed to obtain the tangent modulus, as follows:

$$E_t = \frac{\mathrm{d}\sigma_1}{\mathrm{d}\varepsilon_1} = \frac{A - C\varepsilon_1^2}{\left(A + B\varepsilon_1 + C\varepsilon_1^2\right)^2} \tag{25}$$

The Duncan-Chang E-v model assumes that ε_1 and ε_3 are hyperbolic, and it is derived that $\frac{-\varepsilon_3}{\varepsilon_1}$ and ε_3 are linear, as follows:

$$\frac{-\varepsilon_3}{\varepsilon_1} = F - D\varepsilon_3 \tag{26}$$

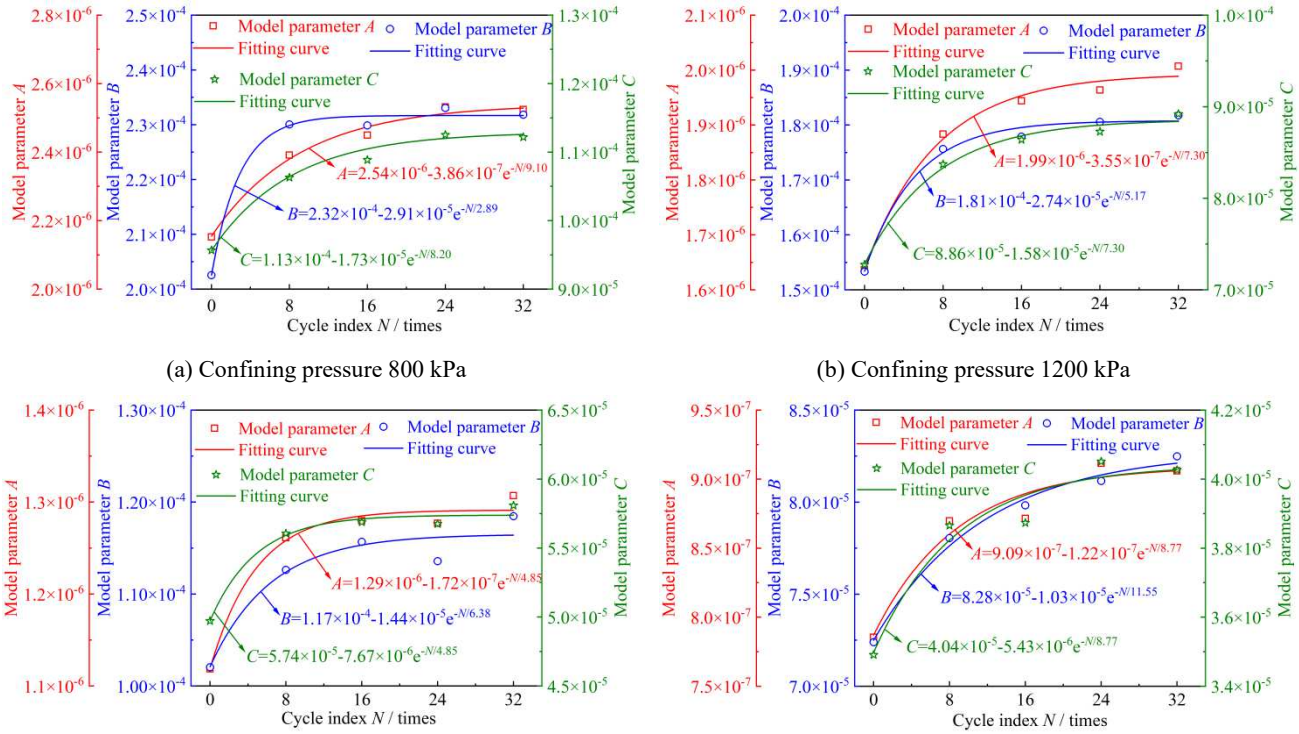
In the formula, F and D are the model parameters.

4.2 Damage evolution of model parameters

Fig. 17 illustrates the variation of the stress-strain model parameters A, B, and C of the modified Duncan-Chang model with increasing dry-wet cycles. As shown in the figure: (1) At a confining pressure of 800 kPa, the model parameters A, B, and C range from 2.0×10^{-6} to 2.8×10^{-6}, 2.0×10^{-4} to 2.5×10^{-6}, and 9.0×10^{-5} to 13.0×10^{-5}, respectively. With increasing confining pressure, these parameters decrease, reaching values between 7.5×10^{-7} and 9.5×10^{-7}, 7.0×10^{-5} and 8.5×10^{-5}, and 3.4×10^{-5} and 4.2×10^{-5}, respectively. (2) The parameters ~~*A, B, and C*~~ showed significant periodic growth characteristics with the increase of the number of dry-wet cycles. At the initial stage, it showed an exponential growth trend, and the growth rate gradually tended to be gentle in the later stage. In the later stages, this increase stabilizes. A functional relationship exists between the model parameters A, B, and C, and the number of dry-wet cycles, which can be expressed by the following formula:

$$A、B、C = Ge^{-N/H} + I \tag{27}$$

In the formula: N is the number of dry and wet cycles; G, H, *and* I are the fitting parameters.



(a) Confining pressure 800 kPa

(b) Confining pressure 1200 kPa

(c) Confining pressure 2000 kPa

(d) Confining pressure 3000 kPa

Fig.17 The curve of model parameters *A*, *B*, *C* with the number of cycles

5 Discussion

Many research results have confirmed that [5-12, 20], the deformation and deterioration process of rockfill is closely related to the dry-wet cycle effect, which has become a key index to evaluate the stability of engineering structures. Therefore, it is very important to systematically explore the variation law of mechanical properties of rockfill materials under dry-wet cycle conditions to ensure the safe operation of engineering structures. At present, although the academic community has explained the evolution mechanism of the macroscopic and microscopic mechanical behavior of rockfill materials under the action of dry-wet cycles to a certain extent by means of physical tests and numerical simulations, the research methods are still dominated by physical tests.The interpretation of micrstructural evolution remains insufficient. This study, based on DEM, conducts triaxial numerical simulations of rockfill under varying dry-wet cycles. It examines the evolution of mechanical properties of rockfill at both macro and micro scales, revealing the internal deformation mechanisms. Compared to previous research, this work offers a more comprehensive description of the microscopic mechanisms corresponding to macroscopic behaviors and provides a novel perspective on the deterioration of the mechanical properties of rockfill materials. Experimental data demonstrate that dynamic reorganization of micr-fabric fundamentally controls macroscopic mechanical responses in rockfill subjected to wetting-drying cycles.

(1) Macroscopic appearance: The results indicate that the number of dry-wet cycles (*N*) significantly impacts the macroscopic mechanical behavior of rockfill, with deformation, peak strength, cohesion, internal friction angle, particle

breakage rate, and particle count decreasing exponentially as N increases. Once N exceeds a certain threshold, the rate of attenuation for these parameters becomes minimal. Under high stress, the particle fracture will be intensified, and the acceleration of the crushing rate and the increase of the number of particles prove to be in stark contrast to the limited evolution under low stress. Moreover, the breakage rate is positively correlated with the accumulated plastic work.

(2) Microscopic mechanism: The underlying mechanism of the observed macroscopic behavior is primarily attributed to the development of fractures, which leads to a reduction in particle strength. However, particle degradation hinges on a critical stress threshold that governs its mechanical behavior. Under low stress, elastic compression—a reversible deformation—and inter-particle dislocation slip along crystallographic planes prevail. These processes generate minor strains, leading to limited particle breakage and a slight increase in particle count as larger grains fragment. Grasping this threshold is essential for monitoring the microstructural evolution of granular materials under stress. As N increases, strong contact force chains concentrate around the broken areas, significantly increasing the number and area of contact points. Additionally, as N progresses, the interparticle friction coefficient decreases, promoting displacement sliding and an increased rate of particle crushing.

(3) Limitations and future work: This study sheds light on the macro-micr evolution mechanism under dry-wet cycles using DEM, although further research is needed. In terms of model accuracy, there are discrepancies between the current four-contour models and laboratory test results, which can be refined through contact parameter calibration and the use of irregular particle models. Regarding material generalizability, conclusions based on a single rockfill type have limited applicability; thus, extending the study to typical materials such as schist and granite, and establishing correlation equations between material properties and deterioration, is essential. Lastly, to address the coupling of time effects, conducting dry-wet cycle-creep tests is critical for understanding the aging deformation mechanism under long-term water-force interactions.

6 Conclusion

This study investigated rockfill materials by conducting numerical simulations of broken triaxial tests under varying dry-wet cycle conditions. The macroscopic mechanical properties and micrscopic evolution mechanisms of the rockfill material across different cycles were analyzed from both macro and micr perspectives. A damage evolution analysis based on the modified deformation model was also performed, the study supports these conclusions:

(1) Macroscopic behavior: The peak stress of rockfill material decreases nonlinearly as the number of dry-wet cycles (N) increases. Once N reaches a certain threshold, the peak stress stabilizes. Dry-wet cycles inhibit shear shrinkage during the initial loading stage and shear expansion during the later stages, with this inhibition becoming stable once N exceeds a specific value. Shear strength, cohesion, and the internal friction angle are all functionally

related to N, decaying exponentially. The particle breakage rate and particle count increase significantly in the early cycles, with smaller increases observed in subsequent cycles. Additionally, the particle breakage rate (B_r) for samples under various N values increases with the accumulation of plastic work (W_p).

(2) Microscopic mechanism: Compared to dry-wet cycles, confining pressure exerts a more pronounced influence on the strength chain density, particle breakage distribution, fracture density, displacement field, and average coordination number. As N increases, the strength chain density, crack density, and average coordination number show an overall upward trend, while the distribution area of particle breakage and the displacement field bulging area expand. However, once N reaches a certain value, these microscopic phenomena evolve at a slower rate, indicating that the mechanical properties of rockfill materials stabilize and no longer deteriorate with further dry-wet cycles.

(3) Damage evolution: The damage evolution is analyzed using the improved Duncan-Chang model, addressing the original model's inadequate depiction of softening. The parameters A, B, and C of the stress-strain model increase exponentially with the number of dry-wet cycles, with a more substantial increase observed in the early stages compared to the later stages. There exists an exponential function relationship between the model parameters A, B, and C, and the number of dry-wet cycles, with the growth rate being faster during the initial stages and slowing down as N increases.

Acknowledge

The authors would like to thank Itasca Consulting Group, America, for the support in providing PFC software.

We thank Bullet Edits Limited for the linguistic editing and proofreading of the manuscript.

Funding

This work was supported by Autonomous Region 'Tianshan Talents' Training Program Young Top Talents Project (Grants Nos. 2023TSYCJU0007); Sponsored by Natural Science Foundation of Xinjiang Uygur Autonomous Region (Grants Nos. 2022D01E45); Xinjiang Uygur Autonomous Region Central Leading Local Science and Technology Development Fund Project (Grants Nos. ZYYD2024CG20); Xinjiang Key Laboratory of Water Conservancy Project Safety and Water Disaster Prevention and Control (Grants Nos. ZDSYS-YJS-2024-46).

Declarations

Conflict of intereat The authors declare that they have no known competing financial interests or personal relationships that could have appeared to influence the work reported in this paper.

Data availability

The data that support the findings of this study are available from the corresponding author upon reasonable request.

References

1. Rahmani H, Panah A K (2020) Effect of particle size and saturation conditions on the breakage factor of weak rockfill materials under one-dimensional compression testing. Geomechanics & engineering 21(4): 315-326. https://doi.org/10.12989/gae.2020.21.4.315
2. Yang X P, Li J, Yang Y S et al (2022) Study on gradation and compaction characteristics of gravels for typical. Rock and Soil Mechanics 43(06): 1607-1616. https://doi.org/10.16285/j.rsm.2021.1405
3. Zhao S L, Yang Z J, Fu X D et al (2023) Shear damage mechanism of coarse-grained materials considering strain localization. Rock and Soil Mechanics 44(01): 31-42. https://doi.org/10.16285/j.rsm.2022.0221
4. Naylor D J, Maranha J R, Neves E M D, et al (1997) Aback-analysis of Beliche dam. Géotechnique 47(2): 221-233.
5. Zhang B Y, Zhang J H, Sun G L (2012) Particle breakage of argillaceous siltstone subjected to stresses and weathering. Engineering Geology 137: 21-28.https://doi.org/10.1016/j.enggeo.2012.03.009
6. Zhang B Y, Zhang J H, Sun G L (2015) Deformation and shear strength of rockfill materials composed of softsilt stones subjected to stress, cyclical drying/wetting and temperature variations. Engineering Geology 190: 87-97.https://doi.org/10.1016/j.enggeo.2015.03.006
7. Zhou W, Hua J J, Chang X L et al (2011) Settlement analysis of the Shuibuya concrete-face rockfill dam. Computers and Geotechnics 38(2): 269-280.https://doi.org/10.1016/j.compgeo.2010.10.004
8. Wu F Q, Qi S W, Lan H X (2005) Mechanismof uplift deformation of the dam foundation of JiangyaWater Power Station, Hunan Province, P. R. China. Hydrogeology Journal 13: 451-466.
9. Alonso E E, Olivella S, Pinyol N M (2005) A review of Beliche dam. Géotechnique 55(4): 267-285.
10. Zhou W, Li S L, Ma G et al (2016) Assessment of the crest cracks of the Pubugou rockfill dam based on parameters back analysis. Geomechanics & Engineering 11(4): 571-585.https://doi.org/10.12989/gae.2016.11.4.571
11. Zhang H, Jing Y, Chen J et al (2022) Characteristics and causes of crest cracking on a high core-wall rockfill dam: a case study. Engineering Geology 297: 106488.https://doi.org/10.1016/j.enggeo.2021.106488
12. Jia Y, Xu B, Desai C S et al (2020) Rockfill particle breakage generated by wetting deformation under the complex stress path. International Journal of Geomechanics 20(10): 04020166.
13. Rahmani H, Panah A K (2020) Effect of particle size and saturation conditions on the breakage factor of weak rockfill materials under one-dimensional compression testing. Geomechanics and Engineering 21(4): 315.https://doi.org/10.12989/gae.2020.21.4.315
14. Sun G L (2009) Studies on shear strength and deformation characteristics of rockfill during weathering. Beijing: Tsinghua University.
15. Theivakularatnam M (2015) Durability of Lightly Stabilised Granular Material Subjected to Freeze-Thaw and Wet-Dry Cycles.Geotechnical Special Publication 1410-1419.https://doi.org/10.1061/9780784479087.127
16. Zhang Q Z, Yuan H N, Zhang Q G et al (2015) Experimental study on deformation characteristics of ro ck-fill material under cyclic drying-wetting. Journal of Hydroelectric Engineering 34(12): 33-41.
17. Zhang B Y, Sun G L, Zhang Z L (2010) Degrading deformation of rockfill materials and its constitutive model. Chinese Journal of Geotechnical Engineering 32(1): 98-103.https://doi.org/CNKI:SUN:YTGC.0.2010-01-018
18. Peng C, Xie Y F, Li A R (2022) Study on Mechanical properties of red sandstone rockfill under dry-we t cycle. Journal of University of South China (Science and Technology) 36(3): 54-59.https://doi.org/10.19431/j.cnki.1673-0062.2022.03.008

19. Zhou W, Cheng J, Zhang G, et al (2021) Effects of wetting–drying cycles on the breakage characteristics of slate rock grains. Rock Mechanics and Rock Engineering 54(12): 6323-6337.https://doi.org/10.1007/s00603-021-02618-5
20. Cheng J L, Zhang G K, Deng S H et al (2024) Effect of cyclic wetting-drying on the crushing strength of rockfill grains with different sizes. Rock and Soil Mechanics 45(S1): 95-105.https://doi.org/10.16285/j.rsm.2023.0792.
21. Cundall P A, Strack O D L (1980) A discrete numerical model for granular assemblies. Géotechnique 30 (3): 331-336.https://doi.org/10.1680/geot.1980.30.3.331
22. Liu Y M, Liu H B, Mao H J (2017) DEM investigation of the effect of intermediate principle stress on particle breakage of granular materials. Computers and Geotechnics 84(4): 58-67.https://doi.org/10.1016/j.compgeo.2016.11.020
23. Xu M, Hong J T, Song E X (2017) DEM study on the effect of particle breakage on the macro-and micro- behavior of rockfill sheared along different stress paths. Computers and Geotechnics Volume 89: 113-127.https://doi.org/10.1016/j.compgeo.2017.04.012
24. Yang G, Liu H L, Zhu G J (2012) Numerical simulation study on wetting deformation of coarse aggregate materials. Journal of Disaster Prevention and Mitigation Engineering 32(05): 535-538+551.https://doi.org/10.13409/j.cnki.jdpme.2012.05.008.
25. Huang X W, Zhou W, Ma G et al (2017) Numerical simulation of rockfill wetting considering deterioration of friction coefficient and bond strength. China Rural Water and Hydropower (9): 125-131.https://doi.org/10.3969/j.issn.1007-2284.2017.09.028
26. Yang R X, Zhang L K, Shi C et al (2025) Mechanical properties and numerical simulation of wetting deformation of rockfill materials. Computational Particle Mechanics 1-16.https://doi.org/10.1007/s40571-025-00969-2
27. Zhao Z H, Song E X (2015) Particle mechanics modeling of creep behavior of rockfill materials under dry and wet conditions. Computers and Geotechnics 68: 137-146.https://doi.org/10.1016/j.compgeo.2015.04.008
28. Wang H, Niu X Q, Ma G et al (2024) Discrete element simulation study on the macro- and micr-mechanical properties of rockfill materials under wetting-drying cycles. Rock and Soil Mechanics 45(S1): 665-676.https://doi.org/10.16285/j.rsm.2023.1139
29. Zhang R H, Zhang L K, Shi C et al (2024) Triaxial numerical simulation study on the mechanical properties of rockfill materials under different boundary conditions. Computational Particle Mechanics 1-20.https://doi.org/10.1007/s40571-024-00855-3
30. Huang Q S, Zhou W, Ma G et al (2020) Experimental and numerical investigation of Weibullian behavior of grain crushing strength. Geoscience Frontiers 11(2): 401-411.https://doi.org/10.1016/j.gsf.2019.07.007
31. Karatza Z, Ando E, Papanicolopulos S A et al (2019) Effect of particle morphology and contacts on particle breakage in a granular assembly studied using X-ray tomography. Granular Matter 21: 1-13.https://doi.org/10.1007/s10035-019-0898-2
32. An N, Ma G, Zhou H et al (2023) DEM investigation of the microscopic mechanism of scale effect of sandy gravel material. Acta Geotechnica 18(3): 1373-1390.https://doi.org/10.1007/s11440-022-01667-6
33. Kuang D M, Long Z L, Ogwu I et al (2022) A discrete element method (DEM)-based approach to simulating particle breakage. Acta Geotechnica 17(7): 2751-2764.https://doi.org/10.1007/s11440-022-01667-6
34. Li S J, Li D, Yu S (2015) micr-parameter Inversion of constitutive model for rockfill materials based on macro experimental data. J Shandong Univ Sci Technol 34(05):20–26. https://doi.org/10.16452/i.cnki.sdkizk.20151027.004
35. Parry R H G (1958) On the yielding of soils (Discussion of paper by Roscoe, Schofield and Wroth)

36. Norihiko M, Sukeo O-Hara (1979) Particle-crushing of a decomposed granite soil under shear stresses. So ils and Foundations 19(3): 1-14.https://doi.org/10.3208/sandf1972.19.3_1
37. Chen T J, Ueng T S (2000) Energy aspects of particle breakage in drained shear of sands. Geotechnique 50(1): 65-72. https://doi.org/10.1680/geot.2000.50.1.65
38. Indraratna B , Salim W (2002) Modelling of particle breakage of coarse aggregates incorporating strength and dilatancy. Proceedings of the Institution of Civil Engineers: Geotechnical Engineering 155(4): 243-25 2. https://doi.org/10.1680/geng.155.4.243.38691
39. Wu X L, Shi B X, Liu S C et al (2022) Large-scale triaxial test of rockfill material considering particle breakage. Science Technology and Engineering 22(2): 749-756. https://doi.org/10.3969/j.issn.1671-1815.20 22.02.041
40. Zhang L K (2018) Research on Static-Dynamic Mechanical Properties and Constitutive Model for the Ma terial of High Rockfill Dams. Urumqi: Xinjiang Agricultural University. https://doi.org/10. 27431/d. cnki. gxnyu. 2018. 000007
41. NG T T (2009) Particle shape effect on macro‐and micro‐behaviors of monodisperse ellipsoids. Interna tional Journal for Numerical and Analytical Methods in Geomechanics 33(4): 511-527.https://doi.org/10.10 02/nag.732
42. Shi X, Zhang J S, Meng F et al (2015) Large-scale triaxial test on modified coarse-grained fillers. Journ al of Central South University (Science and Technology) 46(02): 645-652.
43. Ding X S, Zhang L K, Fan P P (2024) Strength degradation law and nonlinear model of remolded loess under dry-wet freeze-thaw cycles condition. Rock and Soil Mechanics 45(S1):324-336. https://doi.org/10.1 6285/j.rsm.2023.1904

Table 1-4

Table 1 Macroscopic parameters

Table 2 Numerical simulation of micrscopic parameters

Table 3 Test scheme

Table 4 Single-line wetting model

Figure 1-17

Fig.1 3D scanning device

Fig.2 Single-particle model diagram

Fig.3 Sample model generation diagram

Fig.4 The relationship between Weibull distribution parameters and dry-wet cycle

Fig.5 Comparison diagram of the numerical test and the physical test results

Fig.6 The deformation relationship curve of rockfill dry-wet cycle test

Fig.7 The strength relationship curve of rockfill dry-wet cycle test

Fig.8 The relationship between the number of dry-wet cycles and c, φ (3000 kPa)

Fig.9 The relationship between B_r and vertical strain in dry-wet cycle test

Fig.10 The relationship between particle count and vertical strain in dry-wet cycle test

Fig.11 The relationship between B_r and W_p of rockfill under different cycles

Fig.12 Distribution map of contact force chain of filling soil in dry-wet cycle test

Fig.13 Distribution of particle breakage position and fracture position of filling soil in dry-wet cycle test

Fig.14 Displacement distribution of filling particles in dry-wet cycle test

Fig.15 Evolution of coordination number in different positions of dry and wet cycle samples (2000 kPa, $N = 32$)

Fig.16 Evolution curve of average coordination number under dry and wet cycles with different rockfill compaction pressures

Fig.17 The curve of model parameters A, B, C with the number of cycles